해양과학기술논문집 제12권 제2호(2003)
Bull. Mar. Sci. & Tech., 12(2) : 13-24(2003)

BULLETIN OF
RIMST MARINE SCIENCE AND TECHHNOLOGY

Null Broadening With Snapshot-Deficient Covariance Matrices in Passive Sonar

H. Song, *Member, IEEE*, W. A. Kuperman, W. S. Hodgkiss, *Member, IEEE*, Peter Gerstoft, and Jea Soo Kim

***Abstract*—Adaptive-array beamforming achieves high resolution and sidelobe suppression by producing sharp nulls in the adaptive beampattern. Large-aperture sonar arrays with many elements have small resolution cells; interferers may move through many resolution cells in the time required for accumulating a full-rank sample covariance matrix. This leads to "snapshot-deficient" processing. In this paper, the null-broadening technique originally developed for an ideal stationary problem is extended to the snapshot-deficient problem combined with white-noise constraint (WNC) adaptive processing. Null broadening allows the strong interferers to move through resolution cells and increases the number of degrees of freedom, thereby improving the detection of weak stationary signals.**

***Index Terms*—Covariance matrix taper (CMT), null broadening, robust adaptive beamforming, snapshot-deficient processing, white-noise constraint (WNC).**

I. Introduction

RECENT trends in passive sonar systems include the use of large-aperture arrays with many elements to form narrow beams in order to detect quiet targets in a noisy background [1], [2]. This paper is concerned with the detection of weak sources in the presence of fast-moving strong interferers crossing many resolution cells in a time interval too small to build a full-rank covariance matrix. To achieve this, we combine the null-broadening approach developed for an ideal stationary problem [3]–[5] with white-noise constraint (WNC) adaptive processing [6].

At low frequencies, the background often is dominated by loud and fast surface ships that move through many narrow beams or cells in the time it takes to obtain a satisfactory sample covariance matrix. Larger arrays require longer duration snapshots due to the longer transit time of sound across the array. More snapshots are also needed due to the many elements [7]–[10]. Usually, this leads to "snapshot-deficient" processing [1]. A number of techniques have been developed to carry out adaptive processing with less-than-full-rank covariance matrices. The two most common are diagonal loading [11] and subspace methods [12], [13]. Recently, a multirate adaptive beamforming (MRABF) approach was proposed by Cox [2], which uses only a few snapshots to estimate and null the loud moving interferers, followed by more-standard adaptive procedures using many more snapshots to find weak stationary targets.

Null broadening can provide a simple and robust approach to the snapshot-deficient problem arising from the motion of strong interferers when combined with robust WNC processing [6]. Because adaptive-array processing places sharp nulls in the directions of interferers, the presence of interferer motion does not provide sufficient nulling of the interferer given the number of snapshots available, which results in a masking of the desired target signal. Fig. 1 shows an example where source motion degrades the performance with 20 snapshots for a 128-element array, especially on the weakest target at $u = \sin\theta = -0.7$. We also note that the bias of signal and noise has increased significantly due to source motion, which will be discussed in Section II. Null broadening allows the interferers to move through resolution cells while also being contained within a single wide null. In addition, the WNC can exploit the significant bias associated with snapshot deficiency [1].

The null-broadening concept [3]–[5] was originally developed to improve the robustness of the adaptive algorithms and demonstrated for a stationary problem. The potential of this approach, however, has not been fully explored due to its undesirable effects, such as decrease in array gain and broadening of the mainlobe. Here we extend the null-broadening approach to detect weak stationary targets in a nonstationary background such that only a limited number of snapshots are available due to fast-moving strong interferers crossing many resolution cells. Specifically, in this article we

- review adaptive planewave beamforming *vis a vis* snapshot and bias issues;
- describe the null-broadening techniques in terms of eigenvalues;
- demonstrate the robustness of the null-broadening approach combined with the WNC processing for a snapshot-deficient problem arising from source motion in the presence of mismatch;
- investigate the bias issues associated with the processing method;
- characterize the performance of the null-broadening approach using probability of detection.

Manuscript received September 27, 2002; revised April 29, 2003. This work was supported by the Office of Naval Research (ONR) and Defense Advanced Research Projects Agency. This research was motivated by our participation in the ONR Ocean Acoustic Observatory Panel.

H. Song, W. A. Kuperman, W. S. Hodgkiss, and P. Gerstoft are with the Marine Physical Laboratory, Scri Gerstoft are with the Marine Physical Laboratory, Scripps Institution of Oceanography, La Jolla, CA 92093-0238 USA (e-mail: hcsong@mpl.pps Institution of Oceanography, La Jolla, CA 92093-0238 USA (e-mail: hcsong@mpl.ucsd.edu; wak@mpl.ucsd.edu; wsh@mpl.ucsd.edu; gerstoft@mpl.ucsd.edu).

J. S. Kim is with the Division of Ocean System Engineering, Korea Maritime University, Pusan 606-791, South Korea (e-mail: jskim@kmaritime.ac.kr).

Digital Object Identifier 10.1109/JOE.2003.814055

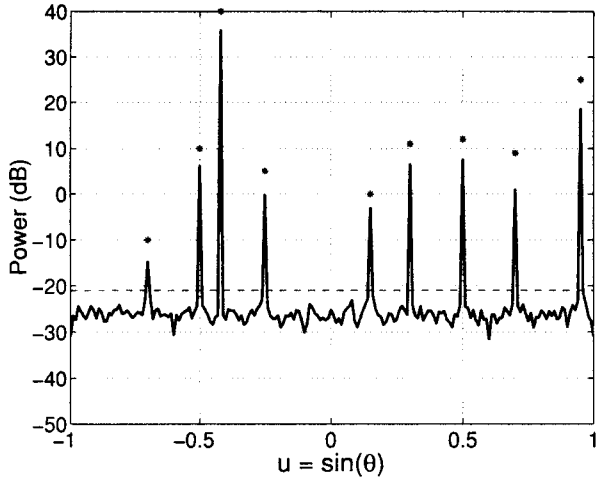

(a)

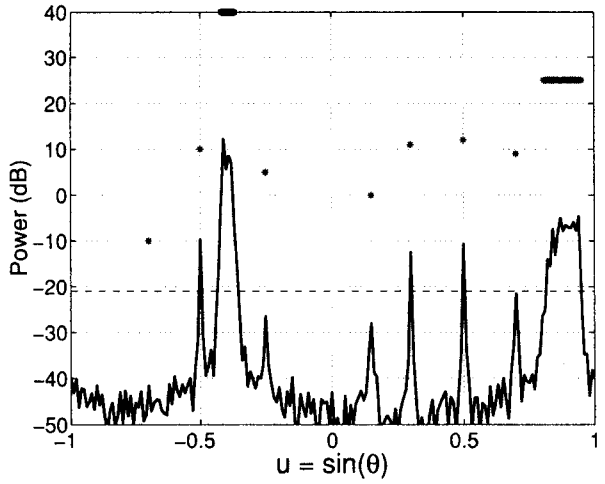

(b)

Fig. 1. Adaptive beamforming with $K = 20$ snapshots for a $N = 128$ element array: (a) 9 fixed sources and (b) 2 moving and 7 fixed sources. The source levels and positions are denoted by $*$. The horizontal dashed line indicates the noise level minus the array gain ($10 \log N$). The effect of source motion over 20 snapshots is observable in (b), especially on the weakest target at $u = \sin\theta = -0.7$. Note that the bias of signal and noise has increased significantly due to source motion, which will be exploited in Section V.

II. Snapshot-Deficient Processing

We begin by briefly reviewing adaptive planewave beamforming (ABF). We then address snapshot-deficient processing due to source motion and discuss the bias issue and nulling of strong interferers.

A. ABF

MVDR adaptive beamforming places nulls in the direction of loud interferers in the acoustic environment described by the cross-spectral density matrix (CSDM) or covariance matrix [2]. The MVDR weights with diagonal loading is

$$\mathbf{w}_{\mathrm{MVDR}}(\theta) = \frac{[\mathbf{R} + \epsilon\mathbf{I}]^{-1}\mathbf{s}(\theta)}{\mathbf{s}^{\dagger}(\theta)[\mathbf{R} + \epsilon\mathbf{I}]^{-1}\mathbf{s}(\theta)} \tag{1}$$

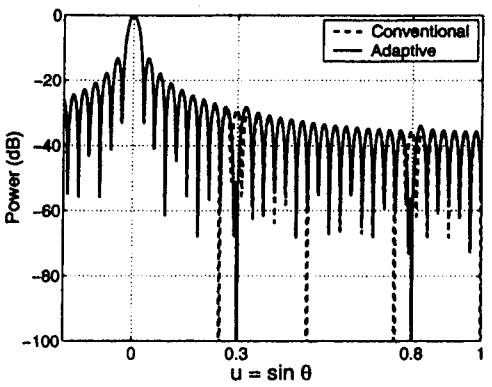

Fig. 2. Beampattern of linear $N = 64$ element array when steered broadside ($\theta = 0$) with interfering sources at $u = 0.3$ and $u = 0.8$: CBF (dashed line) and ABF (solid line). Note the two-deep nulls in the directions of the interferers with ABF.

where $\mathbf{R}$ is the measured covariance matrix, $\mathbf{s}(\theta)$ is the steering vector pointing θ degrees from the broadside, $\dagger$ denotes the Hermitian transpose operation, and $\mathbf{I}$ is the identity matrix. The optional diagonal loading of strength ϵ is included to control the white-noise gain.

Fig. 2 shows the beampattern of a linear array with 64 sensors with half-wavelength spacing ($\lambda/2$) when steered to the broadside $u = 0$. The array is subjected to two stationary interfering sources of the same amplitude and located at $u_1 = \sin(\theta_1) = 0.3$ and $u_2 = \sin(\theta_2) = 0.8$. Note the deep and sharp nulls produced in the directions of two interferers with ABF (solid line) compared to a conventional beampattern in the background (dashed line). The interfering sources are 30 dB louder than the channel noise. The exact, full-rank CSDM without diagonal loading is used for this example such that

$$\mathbf{R} = \sigma_s^2 \left[\mathbf{s}(u_1)\mathbf{s}(u_1)^{\dagger} + \mathbf{s}(u_2)\mathbf{s}(u_2)^{\dagger}\right] + \sigma_n^2\mathbf{I} \tag{2}$$

with $\sigma_s^2 = 30$ dB and $\sigma_n^2 = 0$ dB.

A robust version of the MVDR beamformer is the white-noise gain-constraint (WNC) beamformer [6], which adjusts the diagonal loading ϵ for each steering angle θ to satisfy a white-noise constraint G_w such that

$$\delta^2 < G_w = \left|\mathbf{w}^{\dagger}\mathbf{w}\right|^{-1} < N \tag{3}$$

where N is the number of elements of the array and $\mathbf{w}$ is given by (1). In practice, the white-noise gain (WNG) is introduced as

$$\mathrm{WNG} = 10\log(\delta^2/N) \leq 0 \text{ dB} \tag{4}$$

where WNG $= 0$ dB corresponds to a linear processor and WNG $= -\infty$ dB corresponds to a pure MVDR processor. WNG $= -2$ dB will be used later in the simulations, which is chosen as a compromise in the presence of mismatch in the array-element positions between the robustness of the conventional linear processor and the interference-rejection capability of the pure MVDR processor.

B. Sample Covariance Matrix

The sample covariance matrix is

$$\hat{\mathbf{R}} = \frac{1}{K}\sum_{i=1}^{K} \mathbf{x}_i \mathbf{x}_i^{\dagger} \tag{5}$$

where the $\mathbf{x}_i$ are the complex Fourier-amplitude vectors of the receiver outputs at the frequency of interest and the ith snapshot and K is the number of snapshots.

As discussed by Baggeroer and Cox [1], there are time and bandwidth limits on the number of snapshots available with large-aperture sonar arrays operating in a dynamic environment. At broadside, the mainlobe of a resolution cell has a cross-range extent of

$$\Delta X \approx r\,\frac{\lambda}{L} \tag{6}$$

where r is the range to a source, L is the aperture of the array, and λ is the wavelength. A source moving with tangential speed $v = r\dot{\theta}$ transits this resolution cell and is within the cell for duration

$$\Delta T = \frac{\Delta X}{r\dot{\theta}} \approx \frac{\lambda}{L\dot{\theta}} \tag{7}$$

where $\dot{\theta}$ is the bearing rate of the source.

The limit to the available bandwidth for frequency averaging is determined by signals close to endfire. The estimate of the phase in the cross spectra is smeared when one averages over too large of a bandwidth. The available bandwidth is constrained by [1], [7]

$$B < \frac{c}{8L} = \frac{1}{8T_{\text{transit}}} \tag{8}$$

where $T_{\text{transit}} = L/c$, the transit time across the array at endfire. The product of ΔT and B gives the approximate number of snapshots K available. In this paper, we are primarily concerned with the case when source motion limits the number of snapshots assuming narrow-band signals.

C. Snapshots and Bias

The usual criterion employed in adaptive processing for adequate estimation of $\hat{\mathbf{R}}$ was specified to be $K > 2N$ by Reed *et al.* [9]. This typically is unattainable for most sonar operating environments with multiple moving surface ships representing discrete sources, especially for large arrays with narrow beams. Carlson [11] suggested diagonal loading the sample covariance matrix to reduce the required samples to as few as 1-2 N. Other results [2], [14], [15] suggest that effective nulling can be achieved with K at least equal to twice the number of strong interfering sources M (i.e., $K \geq 2M$ for $N \gg M$).

When using a limited number of snapshots and diagonal loading, significant biases (loss in the estimated output power) are introduced in adaptive processing [1], [7], as seen earlier in Fig. 1. The Capon and Goodman formula for bias and variance [20] is valid only for the case of no loading and with $K \geq N$, which is typically not the case for sonars. An analytical formula is given in [15] for $K > M$ under some conditions on the diagonal loading (i.e., $\sigma_n^2 < \epsilon \ll \lambda_K$ where λ_K denotes the smallest interference eigenvalue).

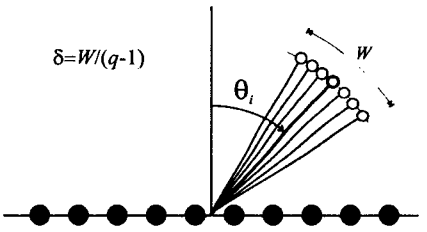

Fig. 3. Mailloux approach [3] distributes a cluster of q equal-strength incoherent sources arranged in a line centered around each source direction θ_i with a trough width of W between the outermost nulls.

Since there are no analytical results for bias in general when $K < N$ with diagonal loading $\epsilon \leq \sigma_n^2$, Baggeroer and Cox [1] showed, via Monte Carlo simulations, two important features: 1) the bias does not depend upon direction and 2) the bias for $K < N$ is significant. In particular, the bias increases with a decrease in the number of snapshots. In the presence of mismatch, however, the bias depends upon direction such that strong signals are subject to much larger signal suppression than are weak signals [16].

It will be shown that the significant bias due to snapshot deficiency turns out to be beneficial because it can be exploited by the WNC processor, which can reduce the bias selectively resulting in a significant increase in dynamic range. The effect of diagonal loading on the bias (MVDR) is described theoretically using eigenanalysis in the Appendix, which confirms that the bias is independent of steering angle as indicated in [1].

III. Null Broadening

In this section, we review the null-broadening approaches [3]–[5] with a focus on the useful property for a snapshot-deficient problem. The method is most simply presented by considering a line array, although it can be applied to two-dimensional planar arrays.

A. Distribution of Fictitious Sources

Assuming that the narrow-band signals impinging on the array are uncorrelated with each other as well as with the spatially white noise, the terms in the covariance matrix $\mathbf{R}$ for a one-dimensional array are [3]

$$R_{mn} = N_n \delta_{mn} + \sum_{l} \sigma_l^2 e^{j(2\pi/\lambda)(x_m - x_n)u_l}. \tag{9}$$

The sum is performed over all interfering sources with averaged power σ_l^2 and direction cosines $u_l = \sin\theta_l$ for θ measured from the broadside. The numbers x_m are the element locations, $\mathbf{N}$ is the noise covariance, and δ_{mn} is a Kronecker delta function.

In order to produce a trough of width W in each of the interference directions u_l, Mailloux [3] distributed a cluster of q equal-strength incoherent sources around each original source, as shown in Fig. 3. In this case, the additional sources can be summed in closed form as a geometric sum and can be written as

$$\sum_{k=1}^{q} \left(\sigma_l^2/q\right) e^{j(2\pi/\lambda)(x_m - x_n)(u_l + k\delta)} = \frac{\sin(q\Lambda_{mn})}{q\sin(\Lambda_{mn})}\,\sigma_l^2 e^{j(2\pi/\lambda)(x_m - x_n)u_l} \tag{10}$$

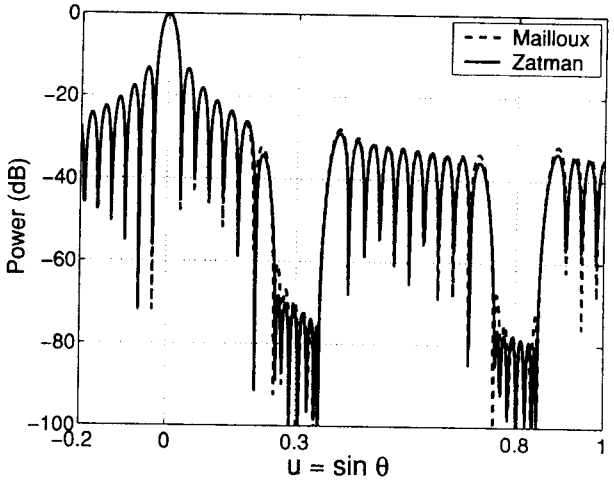

Fig. 4. Beampattern of a $N = 64$ element array steered broadside with augmented covariance matrix $\tilde{\mathbf{R}}$: Mailloux (dashed line) with $q = 7$ and Zatman (solid line). Two interfering sources are incident at $u = 0.3$ and $u = 0.8$. Note the null broadening obtained at these two locations using $W = 0.1$.

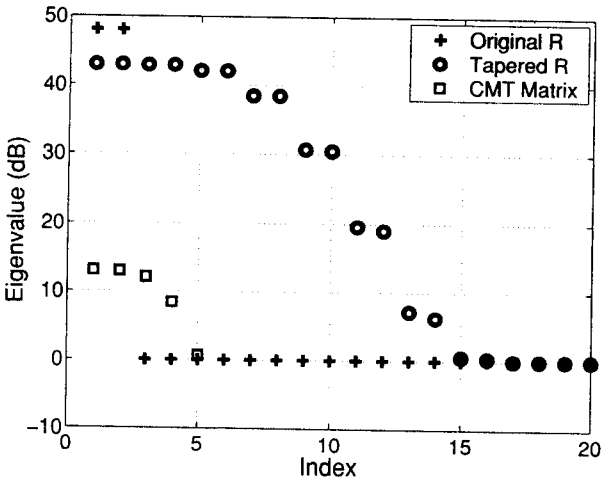

Fig. 5. The eigenvalues of the original covariance matrix $\mathbf{R}$ (crosses) and the tapered matrix $\tilde{\mathbf{R}}$ (circles) for an $N = 64$ element array. The significant number of eigenvalues has increased from 2 to 14. On the other hand, the larger eigenvalues have decreased, resulting from the CMT operation. The first five eigenvalues of the CMT matrix $\mathbf{T}$ are also superimposed (squares).

where $\Lambda_{mn} = \pi(x_m - x_n)\delta/\lambda$ and $\delta = W/(q-1)$. Since there is no angle dependence in the sinc function, we obtain a new covariance matrix term

$$\tilde{R}_{mn} = R_{mn} \frac{\sin(q\Lambda_{mn})}{q\sin(\Lambda_{mn})}. \tag{11}$$

In this formulation, we have introduced a source strength equally distributed with level σ^2/q rather than σ^2 in [3].

In Fig. 4, the adaptive beampattern of a $N = 64$ element linear array is shown with the original covariance matrix $\mathbf{R}$ of (2) replaced by the augmented covariance matrix $\tilde{\mathbf{R}}$ in (11) with $W = 0.1$ and $q = 7$ (dashed line). As opposed to the sharp nulls in Fig. 2, the beampattern clearly shows null broadening.

B. Dispersion Synthesis

Rather than physically distributing fictitious sources, Zatman [4] used dispersion to widen the null of a narrow-band signal. Assuming a rectangular spectrum of bandwidth b_w centered at frequency f_0, the augmentation of the fictitious sources is achieved by a synthetic averaging of the narrow-band covariance matrix $\mathbf{R}(f)$ over the bandwidth

$$\begin{aligned}\tilde{R}_{mn} &= \frac{1}{b_w}\int_{f_0-(b_w/2)}^{f_0+(b_w/2)} R_{mn}(f)\,df \\ &= \frac{\sin(\pi b_w \tau_{mn})}{\pi b_w \tau_{mn}} R_{mn}(f_0)\end{aligned} \tag{12}$$

where $R_{mn}(f) = e^{j2\pi f\tau_{mn}}$ and $\tau_{mn} = (x_m - x_n)u_l/c$ is the time delay between the elements. For actual broad-band signals, null broadening was demonstrated in [17] with experimental data by making use of waveguide invariant theory [18] and averaging the estimated array-covariance matrix across frequency.

For a half-wavelength uniform line array $x_m - x_n = (m-n)\lambda/2$, the wide-band covariance matrix can be calculated as the Hadamard (element-wise) product [19] of $\mathbf{R}$ and $\mathbf{T}$ as

$$\tilde{\mathbf{R}} = \mathbf{R} \circ \mathbf{T} \tag{13}$$

where $T_{mn} = \mathrm{sinc}[(m-n)d]$ and $d = b_w u_l/2f_0 = W/2$ corresponds to half of the null width W defined in the Mailloux approach. The solid line in Fig. 4 shows the resulting beampattern using the wide-band covariance matrix $\tilde{\mathbf{R}}$ with $d = W/2 = 0.05$. It is interesting to note that the bandwidth b_w implicitly varies with the direction cosine $u = \sin\theta$ for a fixed value of d to keep $b_w u$ a constant.

Although both approaches achieve null broadening to the desired width W, note from Fig. 4 that the solid line produces flatter troughs in the adaptive pattern than does the dashed line. Zatman's approach produces continuous fictitious sources distributed along the beamwidth W, whereas the Mailloux approach places a finite number of discrete sources q within the beamwidth. As q increases, the two approaches become identical.

C. Covariance Matrix Taper

Guerci [5] combined the above null-broadening approach with diagonal loading through the concept of a "covariance matrix taper" (CMT) and theoretically investigated the effect of CMT on the adaptive beampattern. In this paper, diagonal loading is handled separately by the robust WNC processor.

The Mailloux–Zatman (MZ) null-broadening approach is described in (13) as a modification of the original sample covariance matrix $\mathbf{R}$ through the CMT matrix $\mathbf{T}$, which is a positive semidefinite matrix with its diagonal entries equal to 1. Note that both $\mathbf{R}$ and $\tilde{\mathbf{R}}$ are, in general, positive semidefinite Hermitian matrices.

Null broadening or the Hadamard operation increases the number of eigenvalues [degrees of freedom (DOF)] such that

$$\mathrm{rank}(\mathbf{R}) \le \mathrm{rank}(\mathbf{R} \circ \mathbf{T}) \le \mathrm{rank}(\mathbf{R}) \times \mathrm{rank}(\mathbf{T}) \tag{14}$$

whose proof can be found in [19] (Theorem 5.1.7). Fig. 5 demonstrates that the two eigenvalues corresponding to each interferer have increased to 14 above the noise level, since each interferer is represented by fictitious nearby sources. For

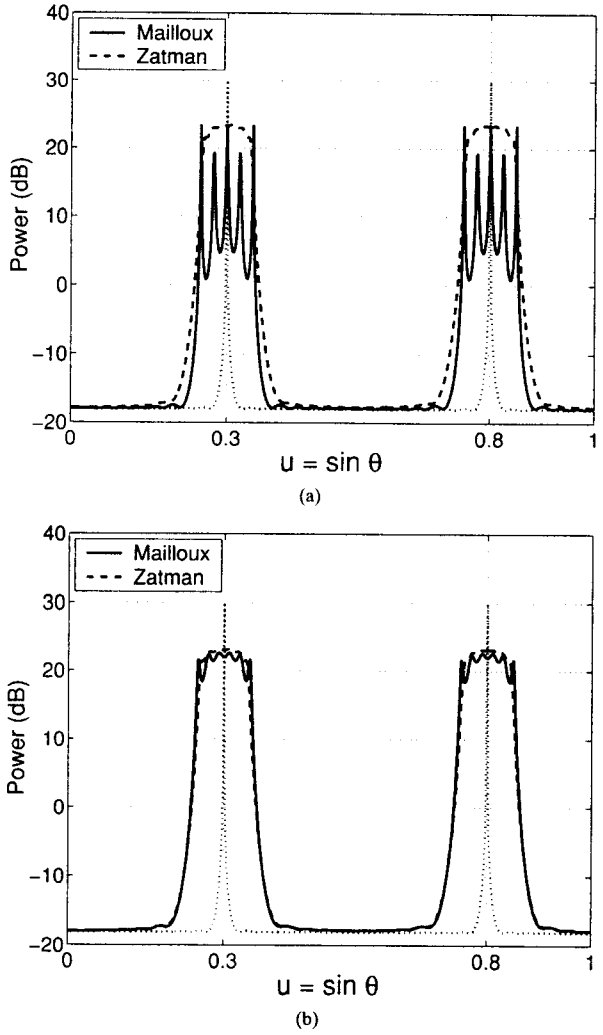

Fig. 6. MVDR output power using the Mailloux approach (solid) with $\tilde{\mathbf{R}}$: (a) $q = 5$ and (b) $q = 7$. The result with the Zatman approach is superimposed in the dashed line. Note that $q < 7$ produces resolvable discrete sources rather than a broad null. The dotted line is the output power with $\mathbf{R}$.

a snapshot-deficient problem, the rank of $\mathbf{R}$ usually is K and is much smaller than the number of array elements N. In this case, the increased degrees of freedom by the null-broadening approach will be significant and can enhance the detection of weak targets in the presence of strong interferers.

The number of significant eigenvalues of the CMT matrix $\mathbf{T}$ is $(W/(\lambda/L) + 1)$ from the analogy between the temporal and spatial domains [21], [22]. This corresponds to the number of resolution cells over the null width W plus one. Fig. 5 shows that there are four significant eigenvalues in $\mathbf{T}$ for $W/(\lambda/L) = 3.2$ (squares). However, the number of fictitious sources distributed over a null width W is determined by the resolution capability of an adaptive beamformer [16], [23]. Fig. 6 shows the MVDR beamformer output power (solid line) when (a) $q = 5$ and (b) $q = 7$. We observe that all of the fictitious sources are resolved when $q = 5$ rather than producing a broad null as shown when $q = 7$, indicating that each resolution cell requires approximately two fictitious sources due to the higher resolution for this example. Note that $q = 7$ corresponds to the number of eigenvalues larger than the noise level (or the effective rank of $\mathbf{T}$) in Fig. 5 (circles) for each source. A lower bound on the angular resolution is derived in [23], applying the Cramer–Rao formalism demonstrating that it is proportional to the classical Rayleigh limit (λ/L) and a factor depending on the output signal-to-noise ratio (SNR).

It is also shown in Fig. 6 that the CMT operation reduces the beamformer output power due to discrete sources since it distributes the source power over the null width W. However, the reduction of the signal power is negligible as compared to the significant bias resulting from a small number of snapshots when applied to a snapshot-deficient problem, as discussed in Section II-C. Note that the total power is preserved since the trace of $\mathbf{R}$ is not affected by the CMT matrix $\mathbf{T}$, whose diagonal entries are equal to 1. Accordingly, the largest eigenvalues of the original covariance $\mathbf{R}$ (crosses) have decreased in $\tilde{\mathbf{R}}$ (circles) in Fig. 5.

IV. Null Broadening With Snapshot Deficient $\hat{\mathbf{R}}$

Thus far, the null-broadening technique has been applied to either an exact covariance matrix $\mathbf{R}$ in (9) or to a 2 N sample covariance matrix by Guerci [5] assuming a stationary process. While the concept was originally introduced for robustness of adaptive algorithms, the usefulness of this approach was limited by its undesirable effects, such as decrease in array gain and broadening of the mainlobe as shown in Fig. 6. Here, we apply the CMT null-broadening approach to the case when only a limited number of snapshots are available due to interference motion (i.e., $K \ll N$) and the interference can move across several resolution cells.

As described in Section II, the number of snapshots is limited by the resolution cell size λ/L. On the other hand, effective nulling of the strong moving interferers usually requires a larger number of snapshots (e.g., at least $K \geq 2M$), where M is the number of sources [1], [14], [15]. Null broadening offers a robust approach to this snapshot-deficient problem. It allows the interferers to move through several resolution cells in the total observation time, increasing the number of snapshots K, usable for weak target detection. At the same time, null broadening increases the DOF by generating fictitious sources over the null width, which the processor uses efficiently by containing each moving source in a single broad null. The increased DOF enables us to detect weak stationary targets otherwise obscured by the strong moving interferers. With the null-broadening approach, we can resolve all of the targets simultaneously, including the moving sources, rather than trying to separate them in a multistage process [2], [12], [13]. This approach is simple because it requires only the Hadamard multiplication without any significant effort. Finally, the previously unexplored benefit of null broadening combined with the WNC adaptive processing is a significant increase in dynamic range by selectively reducing the bias from the small number of available snapshots.

It is appropriate to mention how the value of W is chosen for null broadening in (13). For a stationary problem with an exact covariance matrix $\mathbf{R}$, W is the desirable null width in direction cosine (see Fig. 4). With source motion, we expect to

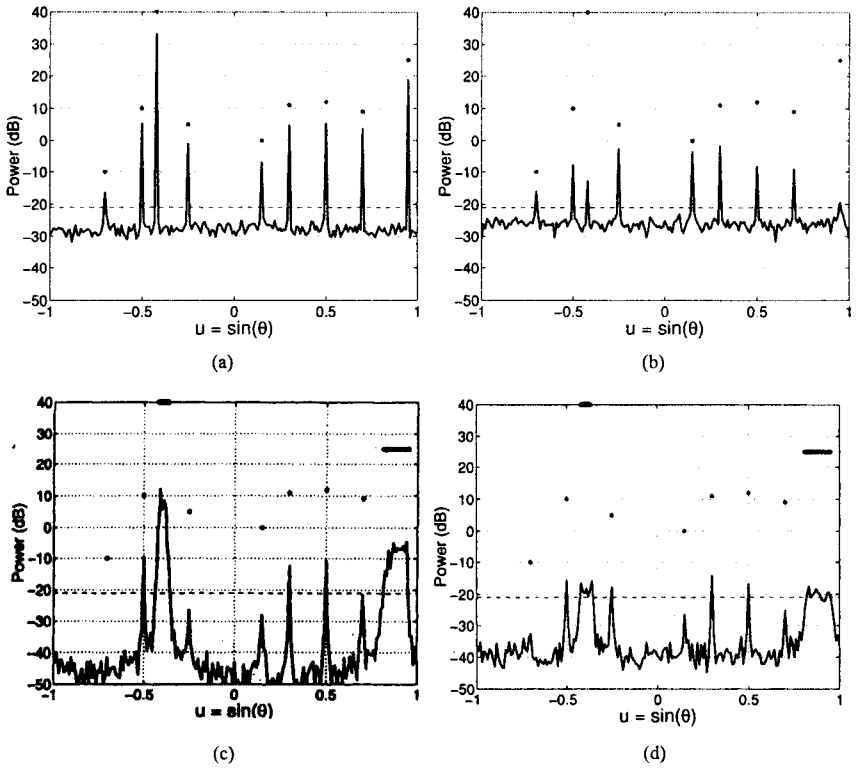

Fig. 7. Baseline results using MVDR processing for $N = 128$, $K = 20$ and diagonal loading of $\epsilon = 10$ dB: (a) nine fixed sources, (b) nine fixed sources with AEL errors, (c) two moving and seven fixed sources, and (d) two moving and seven fixed sources with AEL errors. The source levels and positions are denoted by $*$. The effects of source motion over $K = 20$ snapshots are observable in (c) and (d), especially on the weakest target at $u = -0.7$. Note the bias of MVDR due to the small number of snapshots accumulated.

achieve null broadening with a smaller W rather than the one normally required for a stationary case. In addition, a smaller null width is desirable to resolve closely spaced beams. We will use the notation of W_M to distinguish it from the stationary case. According to our simulations, it appears that a resolution cell size λ/L is appropriate for W_M, although this requires further investigation. It should be noted, however, that we can use quite a broad range of W_M (e.g., $W_M < W$), making null broadening a robust process.

V. Simulations

We test the null-broadening technique using an example with severe motion [2]. However, we increase the number of array elements for snapshot-deficient processing with a smaller resolution cell size.

A. Baseline Results With MVDR Processing

A 128-element linear array with a half wavelength spacing ($N = 128$) is used with a resolution cell size of $\lambda/L = 0.016$. There are two strong moving sources and seven fixed sources ($M = 9$) in 0 dB uncorrelated noise. The source levels are: moving sources (40, 25 dB) and fixed sources (-10, 10, 5, 0, 11, 12, 9 dB). One of the moving sources (25 dB) is initially near endfire ($u = 0.95$) and moves toward broadside with $\Delta u = -0.0075$ per snapshot. The other stronger moving source (40 dB) is initially at $u = -0.42$ with $\Delta u = 0.0028$ (three times slower than the 25-dB source). Doppler frequency shift due to source motion is not taken into account assuming tangential motion. The seven fixed sources are at $u = (-0.7, -0.5, -0.25, 0.15, 0.3, 0.5, 0.7)$ with the weakest target at $u = -0.7$. For these simulations, a mismatch in the array element location (AEL) of 0.1λ rms is introduced, with the exception of Fig. 7(a) and (c).

We use $K = 20$ snapshots, which is about twice the number of sources ($M = 9$) as suggested in [1], [14], and [15]. The two moving sources then occupy 9 and 3 resolution cells, respectively. Fig. 7 shows baseline results obtained using the MVDR processor where the effect of source motion is clearly demonstrated. Note that Fig. 7(a) and (c) are identical to Fig. 1(a) and (b), as shown earlier. A diagonal loading of $\epsilon = 10$ dB is applied, which is 10 dB above the noise level. The source levels and positions are denoted by the asterisks. Fig. 7(a) assumes all nine sources to be stationary, verifying that $K = 20$ snapshots can resolve all of the sources.

Once source motion is introduced in Fig. 7(c), $K = 20$ is not sufficiently large to enable detecting the weakest target at $u = -0.7$. This is because the source motion effectively generates additional sources (e.g., two sources per resolution cell), which in turn require more snapshots at a rate faster than the accumulation of snapshots, thus exceeding the available DOF. Thus the effective number of snapshots is reduced by source

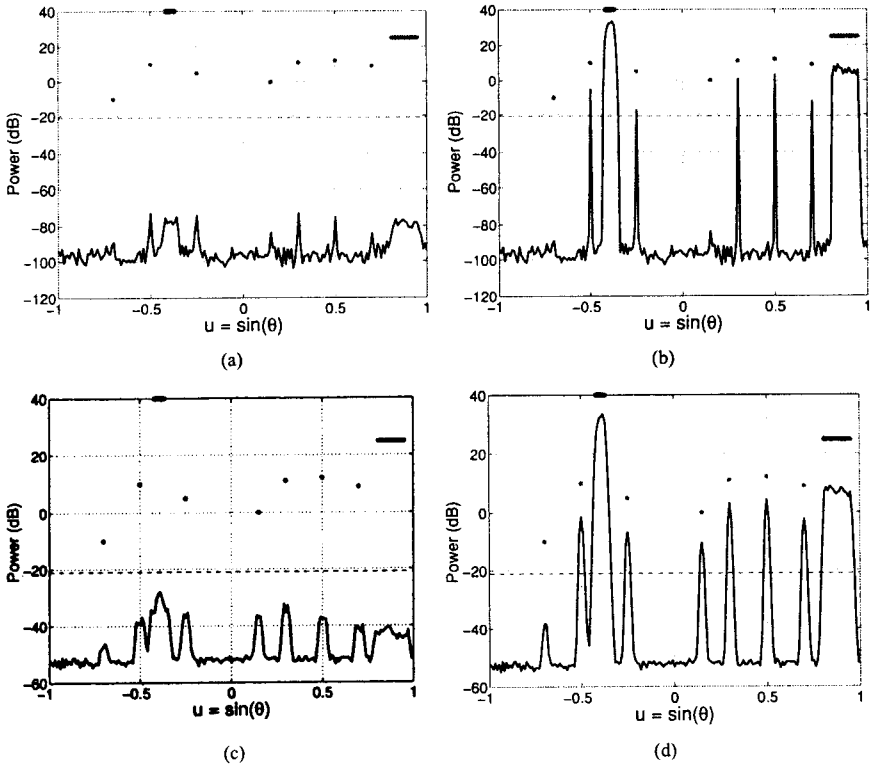

Fig. 8. Adaptive processing with the sample covariance matrix $\hat{\mathbf{R}}$ (upper panels) and a tapered $\tilde{\mathbf{R}}$ (lower panels): (a) MVDR with $\hat{\mathbf{R}}$, (b) WNC with $\hat{\mathbf{R}}$, (c) MVDR with $\tilde{\mathbf{R}}$, and (d) WNC with $\tilde{\mathbf{R}}$. A diagonal loading of $\epsilon = -20$ dB is applied to the MVDR and as a reference level (minimum) to the WNC with WNG $= -2$ dB. Although both (c) and (d) demonstrate the effectiveness of the null-broadening approach over (a) and (c), the WNC processing with $\tilde{\mathbf{R}}$ in (d) shows remarkable performance over MVDR processing with $\tilde{\mathbf{R}}$ in (a) in the presence of AEL errors. Note in (b) and (d) that the bias associated with discrete sources is significantly reduced by the WNC while the noise floor remains the same, resulting in a significant increase in the dynamic range.

motion, resulting in a larger bias in Fig. 7(c), as discussed in Section II. In the presence of 0.1λ rms AEL error, the MVDR results get worse due to its sensitivity to mismatch as shown in Fig. 7(b) and (d), especially for the strong signals (40, 25 dB) subject to larger signal suppression [16]. Next, we combine the null-broadening approach with robust WNC processing to improve the results shown in Fig. 7(d).

B. Null Broadening With Robust WNC Processing

Fig. 8 shows results with the original sample covariance matrix $\hat{\mathbf{R}}$ (upper panels) and a tapered $\tilde{\mathbf{R}}$ (lower panels) with $W_M = 0.013$, respectively. The left and right panels employ MVDR and WNC processing, respectively. Note that Fig. 8(a) is identical to Fig. 7(d), except that diagonal loading of $\epsilon = -20$ dB applied rather than 10 dB. The result is that the noise floor level has decreased from -40 dB to -100 dB, i.e., twice the change in diagonal loading (-30 dB), which will be discussed below. The idea is to apply a diagonal loading that is minimal but sufficient for matrix inversion, allowing the WNC processor to obtain an optimal diagonal loading level subject to the WNG constraint (WNG $= -2$ dB).

Clearly, Fig. 8(c) and (d) demonstrates the effectiveness of the null-broadening approach over (a) and (b), while the beams are broader than Fig. 8(a) and (b). In particular, the WNC processing in Fig. 8(d) shows the best performance in the presence of AEL errors for the weakest target at $u = -0.7$. Note that the WNC processing significantly reduces the bias associated with the discrete sources (compare the left and right panels) without affecting the noise level. As a result, the dynamic range has increased significantly. Another observation is that the noise floor level has increased from -100 dB (upper panels) to -50 dB (lower panels) due to the null broadening. This is because the null broadening increases the DOF or the effective number of snapshots, resulting in a smaller bias [1].

As discussed in Section III-C, null broadening increases the number of degrees of freedom as shown in Fig. 9(a). For $K = 20$, the number of eigenvalues in the sample covariance matrix $\hat{\mathbf{R}}$ is 20. As a result of the Hadamard operation, the significant number of eigenvalues in $\tilde{\mathbf{R}}$ has increased up to 50, counting the eigenvalues down to the 0-dB noise level. Fig. 9(b)–(d) displays the WNC processing results with $\tilde{\mathbf{R}}$ where the first 20, 50, and 100 eigenvectors, respectively, have been included in the processing. In particular, Fig. 9(b) indicates that the first 20 eigenvectors do not represent all the discrete sources as compared to Fig. 9(d) containing 100 eigenvectors, while the best performance in Fig. 9(c), with 50 eigenvectors, confirms the number of significant eigenvalues mentioned above. Note the apparent improvement in the SNR [e.g., from 15 dB in Fig. 9(d) to 26 dB for the weak target at $u = -0.7$] since the noise-floor level is further suppressed by excluding the noise components, despite a slight reduction in the signal power.

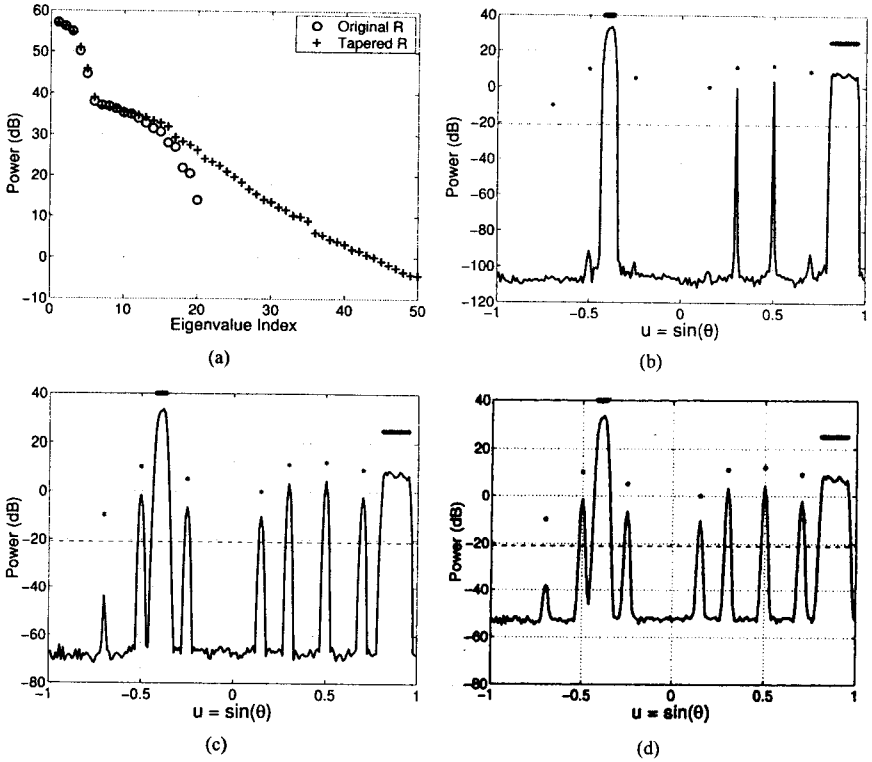

Fig. 9. (a) The eigenvalues of the original covariance matrix $\hat{\mathbf{R}}$ (circles) with $K = 20$ snapshots and the tapered matrix $\tilde{\mathbf{R}}$ (crosses) for an $N = 128$ element array. Plots (b)–(d) show the WNC processing results with $\tilde{\mathbf{R}}$ where the number of eigenvectors included in the processing are 20, 50, and 100, respectively. In particular, (b) indicates that the first 20 eigenvectors do not represent all of the discrete sources as compared to (d), containing 100 eigenvectors. Note that (c), with 50 significant eigenvectors, shows an improvement in the apparent SNR because the noise floor level is further down by excluding the noise eigenvectors.

C. *Effect of Diagonal Loading*

Fig. 10 illustrates the effect of the reference (minimum) level of diagonal loading on the bias for WNC processing with the first 50 eigenvectors: (a) $\epsilon = -30$ dB; (b) $\epsilon = -20$ dB; and (c) $\epsilon = 0$ dB. Fig. 10(d) displays the power of signal at $u = -0.7$ (circles) and the noise (diamonds) as a function of the reference diagonal-loading level where the signal power using MVDR processing (squares) is superimposed for comparison and the noise power (diamonds) is the same for both WNC and MVDR processing. For $\epsilon \leq -10$ dB, the noise power (diamonds) is reduced arbitrarily by the reference level of diagonal loading ϵ with a slope of 2. On the other hand, the WNC signal power (circles) remains the same because the WNC processing increases the diagonal loading from the reference level until it satisfies the WNG constraint WNG $= -2$ dB in (4). The actual level of diagonal loading obtained is $\epsilon_a \approx -10$ dB. As a result, we can increase the dynamic range arbitrarily by using a reference diagonal-loading $\epsilon < -10$ dB with the WNC processing.

The slope of 2 is derived in the Appendix, which applies when the diagonal loading is much smaller than the smallest eigenvalue. The 50th smallest eigenvalue is about -5 dB in Fig. 9(a), which is well above $\epsilon = -10$ dB. As ϵ continues to increase (i.e., $\epsilon > -10$ dB), the slope of both signal and noise approaches 1, as described in the Appendix. The increase in the reference level of diagonal loading above $\epsilon = -10$ dB deprives the WNC processing of its sensitivity controlled by the WNG constraint, turning back to the MVDR processing. We also note that the output power with MVDR (dotted and dashed lines) demonstrates that the bias is independent of steering angle, as indicated in [1]. However, the WNC depends strongly on the steering angle.

D. *Beampattern and Null Width*

Fig. 11 displays the beampattern for WNC processing when steered in the direction of the weakest target at $u = -0.7$. The dashed and solid lines show the results with the original $\hat{\mathbf{R}}$ and the tapered $\tilde{\mathbf{R}}$, respectively. Source positions over the $K = 20$ snapshots are denoted by $*$, not the actual level. For convenience, the dashed curve is displaced by 15 dB. Note the null broadening achieved with $\tilde{\mathbf{R}}$ with respect to the average sidelobe level, especially around the stronger moving interferer at $u = -0.4$. These beampatterns explain why Fig. 8(d) detects the weak target while Fig. 8(b) does not.

In our example, over $K = 20$ snapshots the two moving sources (40 and 25 dB) traversed $W = 0.056$ and 0.15, occupying 3 and 9 resolution cells, respectively. We have used the value of $W_M = 0.013$, corresponding approximately to a resolution cell size $\lambda/L = 0.016$ as discussed in Section IV. Fig. 11 shows that we obtain an effective null width of $W_{\text{eff}} = 0.1$ around the strong moving interferer at $u = -0.4$, which is about 10 times larger than the null width employed W_M.

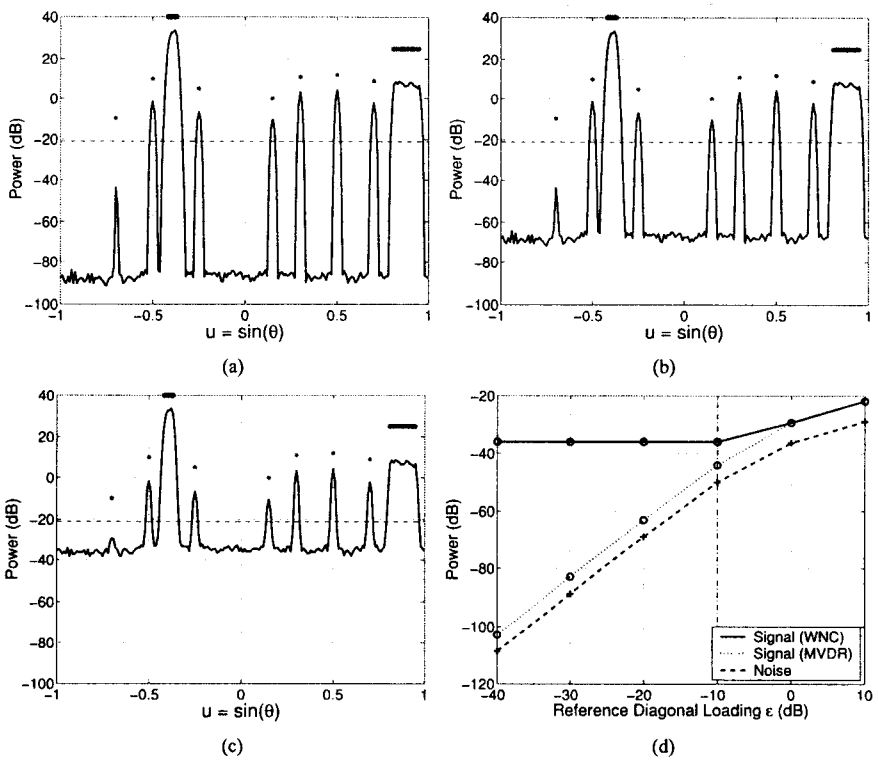

Fig. 10. Effect of the reference (minimum) level of diagonal loading on the bias for WNC processing with the first 50 eigenvectors: (a) $\epsilon = -30$ dB; (b) $\epsilon = -20$ dB; and (c) $\epsilon = 0$ dB. Plot (d) displays the power of the signal at $u = -0.7$ (circles) and noise (diamonds) as a function of the reference diagonal-loading level ϵ, where the MVDR signal power (squares) is superimposed for comparison. Note that the noise power (diamonds) can be reduced arbitrarily with a slope of 2 up to $\epsilon = -10$ dB (see the Appendix) while the WNC signal power (circles) remains the same with a large diagonal loading subject to the WNG constraint WNG $= -2$ dB.

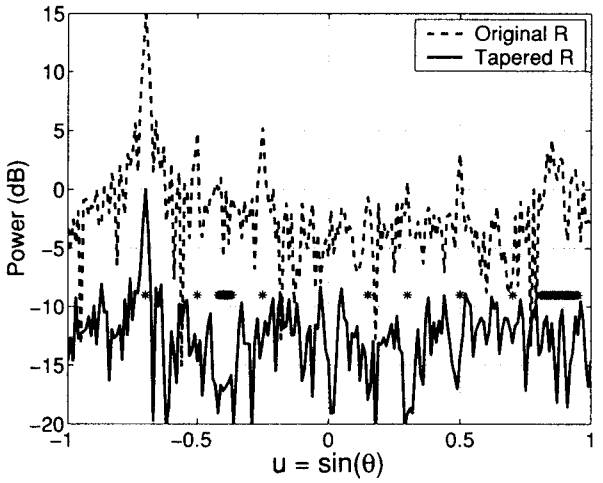

Fig. 11. Adaptive beampattern for WNC when steered in the direction of the weakest target at $u = -0.7$. The dashed and solid lines show the result with the original $\hat{\mathbf{R}}$ and tapered $\tilde{\mathbf{R}}$, respectively. For convenience, the dashed curve is displaced by 15 dB. Source positions over the $K = 20$ snapshots are denoted by $*$, not the actual level. Note the null broadening obtained with $\tilde{\mathbf{R}}$, especially around the strong moving source ($u = -0.4$), with respect to the average sidelobe level.

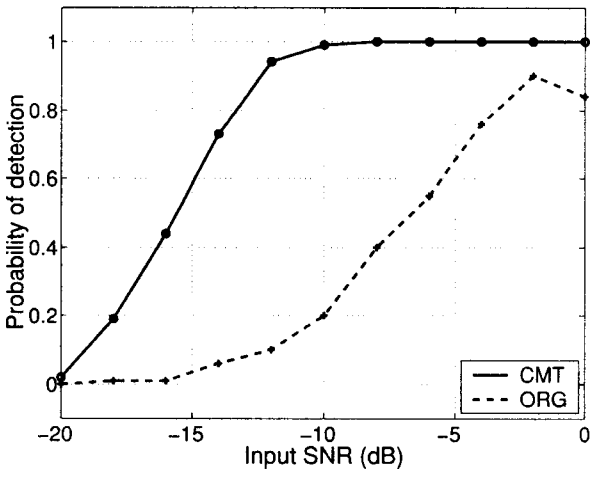

Fig. 12. Probability of detection of the weakest target at $u = -0.7$ as a function of the input SNR for the tapered $\tilde{\mathbf{R}}$ (solid) and original $\hat{\mathbf{R}}$ (dashed).

E. Performance Analysis

The examples so far were based on single trials. Now we characterize the performance of the null-broadening method over 200 independent trials as a function of the input SNR of the weakest target at $u = -0.7$. The performance metric is the probability of detecting, (P_D) the weakest target [see Fig. 8(b) and (d)], when using a high threshold ($P_F \simeq 0$). Fig. 12 shows that the null-broadening approach with $\tilde{\mathbf{R}}$ has a significantly better performance than the case with $\hat{\mathbf{R}}$. Although not shown here, all of the remaining sources are always detected in the

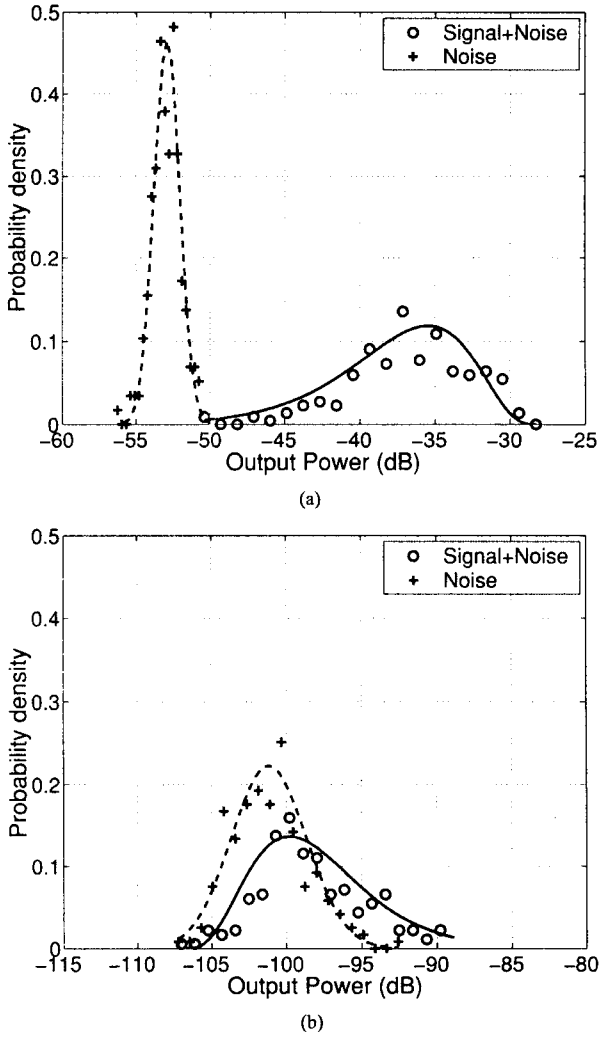

Fig. 13. Probability densities of the signal plus noise (circles and solid line) and the noise alone (crosses and dashed line) for an input SNR $= -10$ dB: (a) tapered $\tilde{\mathbf{R}}$ and (b) original $\hat{\mathbf{R}}$.

null-broadening approach. However, detection of the weakest target with $\hat{\mathbf{R}}$ does not necessarily mean that we can detect all of the other sources, even with an increase in SNR, indicating that we simply do not have enough DOF to detect all of the sources given the number of snapshots. When we plot the probability of detecting all of the sources rather than the single weakest target, the solid line remains the same, while the dashed line gets much worse.

To specify the performance more completely, Fig. 13 shows the probability densities of the signal plus noise (circles) and the noise alone (crosses) from the 200 independent trials when the input SNR $= -10$ dB. Fig. 13(a) shows that the probability of false alarm P_F is almost zero due to separation between the signal-plus-noise and noise-alone densities. On the other hand, Fig. 13(b) shows that there is significant overlap between them, such that the probabilities of detection P_D and false alarm P_F depend on the threshold. For instance, when we choose -95 dB as a threshold, P_D is less than 0.2 for $P_F \simeq 0$.

VI. Conclusion

The null-broadening technique combined with robust WNC adaptive processing has been extended to the snapshot-deficient problem arising from source motion. Null-broadening allows the moving interferers to move through resolution cells and increases the usable number of snapshots. At the same time, it increases the number of degrees of freedom, providing effective nulling of the moving interferers. Thus, the null-broadening approach can improve the detection of weak signals usually obscured by power spreading of the strong moving interferers. In addition, the significant bias introduced in adaptive processing with a small number of snapshots can be exploited by robust WNC adaptive processing, which reduces the bias associated with discrete sources, leaving the biased (low) noise-floor level untouched. The net effect is to increase the dynamic range significantly. Simulations demonstrated the robustness of the null-broadening approach, even with severe interferer motion in the presence of AEL errors.

Appendix
Power Output Versus Diagonal Loading

This appendix derives the quadratic dependence of the MVDR power output on the diagonal-loading level for a covariance matrix $\mathbf{R}$ less than full rank in a snapshot-deficient problem when the diagonal loading is much smaller than the eigenvalues of $\mathbf{R}$.

Consider the eigen-decomposition of $\mathbf{R}$ with a dimension N for a snapshot-deficient problem with $K < N$ snapshots

$$\mathbf{R} = \sum_{i=1}^{K} \lambda_i \mathbf{v}_i \mathbf{v}_i^\dagger \tag{15}$$

where λ_i, $\mathbf{v}_i$ denotes the ith largest eigenvalue and eigenvectors, respectively. Then the inverse of $\mathbf{R}$, with diagonal-loading ϵ, can be written explicitly as [24]

$$[\mathbf{R} + \epsilon \mathbf{I}]^{-1} = \epsilon^{-1} \left[\mathbf{I} - \sum_{i=1}^{K} \left(\frac{\lambda_i}{\lambda_i + \epsilon} \right) \mathbf{v}_i \mathbf{v}_i^\dagger \right]. \tag{16}$$

Substituting this expression into (1), we obtain the MVDR weight vector

$$\mathbf{w}(\mathbf{s}) = \frac{\mathbf{s} - \sum_{i=1}^{K} \beta_i (\mathbf{v}_i^\dagger \mathbf{s}) \mathbf{v}_i}{|\mathbf{s}|^2 - \sum_{i=1}^{K} \beta_i |\mathbf{v}_i^\dagger \mathbf{s}|^2} \tag{17}$$

where $\beta_i = \lambda_i / (\lambda_i + \epsilon)$ and $\mathbf{s}$ is a steering vector.

The output power is

$$P(\mathbf{s}) = \mathbf{w}^\dagger \mathbf{R} \mathbf{w} = \frac{\sum_{i=1}^{K} \lambda_i |\mathbf{v}_i^\dagger \mathbf{s}|^2 (1 - \beta_i)^2}{\left[|\mathbf{s}|^2 - \sum_{i=1}^{K} \beta_i |\mathbf{v}_i^\dagger \mathbf{s}|^2 \right]^2}. \tag{18}$$

Defining $\gamma_i = \lambda_i/(\lambda_i+\epsilon)^2$, we can rewrite the above expression as

$$P(\mathbf{s}) = \epsilon^2 \left[\frac{\sum_{i=1}^{K} \gamma_i |\mathbf{v}_i^\dagger \mathbf{s}|^2}{\left[|\mathbf{s}|^2 - \sum_{i=1}^{K} \beta_i |\mathbf{v}_i^\dagger \mathbf{s}|^2 \right]^2} \right]. \quad (19)$$

When ϵ is much smaller than the smallest eigenvalue λ_K (i.e., $\epsilon \ll \lambda_K$), the effect of ϵ that appears along with λ_i in both β_i and γ_i will be negligible. In this case, the output power P changes quadratically with the diagonal-loading ϵ, i.e., $P \propto \epsilon^2$ resulting in a slope of 2 on a decibel scale. This result confirms that the bias is independent of the steering vector s as indicated in [1].

With $\epsilon \geq \lambda_K$, however, only the eigenvalues comparable to ϵ, i.e., $\lambda_i \approx \epsilon$, will influence the power P. Then $\gamma_i \propto \epsilon^{-1}$ and when ϵ^2 is multiplied with γ_i in the numerator, we end up with a scale factor of ϵ. As a result, the power P is linearly proportional to the diagonal-loading level ϵ.

ACKNOWLEDGMENT

The authors thank Dr. P. Hursky of the Science Applications International Corporation for pointing to the reference by Guerci and A. Baggeroer of the Massachusetts Institute of Technology for a helpful discussion on the performance metric.

REFERENCES

[1] A. B. Baggeroer and H. Cox, "Passive sonar limits upon nulling multiple moving ships with large aperture arrays," in *Proc. IEEE 33rd Asilomar Conf. Signals, Systems Comput.*, Pacific Grove, CA, Oct. 1999, pp. 103–108.

[2] H. Cox, "Multi-rate adaptive beamforming (MRABF)," in *Proc. IEEE Sensor Array Multichannel Signal Processing Workshop*, Cambridge, MA, Mar. 2000, pp. 306–309.

[3] R. J. Mailloux, "Covariance matrix augmentation to produce adaptive array pattern troughs," *Electron. Lett.*, vol. 31, no. 25, pp. 771–772, 1995.

[4] M. Zatman, "Production of adaptive array troughs by dispersion synthesis," *Electron. Lett.*, vol. 31, no. 25, pp. 2141–2142, 1995.

[5] J. R. Guerci, "Theory and application of covariance matrix tapers for robust adaptive beamforming," *IEEE Trans. Signal Processing*, vol. 47, pp. 977–985, Apr. 1999.

[6] H. Cox, R. Zeskind, and M. Owen, "Robust adaptive beamforming," *IEEE Trans. Acoust., Speech, Signal Processing*, vol. 35, pp. 1365–1376, June 1987.

[7] D. E. Grant, J. H. Gross, and M. Z. Lawrence, "Cross-spectral matrix estimation effects on adaptive beamformer," *J. Acoust. Soc. Amer.*, vol. 98, no. 1, pp. 517–524, 1995.

[8] T. R. Meserschmitt and R. A. Gramann, "Evaluation of the dominant mode rejection beamformer using reduced integrated times," *IEEE J. Oceanic Eng.*, vol. 22, pp. 385–392, Apr. 1997.

[9] I. S. Reed, J. D. Mallat, and L. E. Brennan, "Rapid convergence rate in adaptive arrays," *IEEE Trans. Aerosp. Electron. Syst.*, vol. AES-10, pp. 853–863, Nov. 1974.

[10] D. M. Boroson, "Sample size considerations for adaptive arrays," *IEEE Trans. Aerosp. Electron. Syst.*, vol. AES-16, Nov. 1980.

[11] B. D. Carlson, "Covariance matrix estimation errors and diagonal loading in adaptive arrays," *IEEE Trans. Aerosp. Electron. Syst.*, vol. 24, pp. 397–401, July 1988.

[12] I. P. Kirsteins and D. W. Tufts, "On the probability density of signal-to-noise ratio in improved adaptive detector," in *Proc. ICASSP*, Tampa, FL, Mar. 1985, pp. 572–575.

[13] N. L. Owsley, "Enhanced minimum variance beamforming," in *Underwater Acoustic Data Processing*, Y. Chan, Ed. Boston, MA: Kluwer, 1989, NATO ASI series.

[14] J. E. Hudson, *Adaptive Array Principles*. New York: Peregrinus, 1981.

[15] C. H. Gierull, "Performance analysis of fast projections of the Hung–Turner type for adaptive beamforming," *Signal Process.*, vol. 50, pp. 17–28, 1996.

[16] H. Cox, "Resolving power and sensitivity to mismatch of optimum array processors," *J. Acous. Soc. Amer.*, vol. 54, no. 3, pp. 771–785, 1973.

[17] J. S. Kim, W. S. Hodgkiss, W. A. Kuperman, and H. C. Song, "Null-broadening in a waveguide," *J. Acous. Soc. Amer.*, vol. 112, no. 1, pp. 189–197, 2002.

[18] G. A. Grachev, "Theory of acoustic field invariants in layered waveguide," *Acoust. Phys.*, vol. 39, no. 1, pp. 33–35, 1993.

[19] R. A. Horn and C. R. Johnson, *Topics in Matrix Analysis*. New York: Cambridge Univ. Press, 1991.

[20] J. Capon and N. R. Goodman, "Probability distributions for estimators of the frequency wavenumber spectrum," *Proc. IEEE*, vol. 58, pp. 1785–1786, Oct. 1970.

[21] D. Slepian and H. O. Pollak, "Prolate spheroidal wave functions, Fourier analysis and uncertainty," *Bell Syst. Tech. J.*, vol. 40, pp. 43–64, 1961.

[22] H. L. Van Trees, *Detection, Estimation and Modulation Theory, Part I*. New York: Wiley, 1970, pp. 192–194.

[23] A. B. Baggeroer, W. A. Kuperman, and H. Schmidt, "Matched field processing: Source localization in correlated noise as an optimum parameter estimation problem," *J. Acous. Soc. Amer.*, vol. 83, no. 2, pp. 571–578, 1988.

[24] H. Cox and R. Pitre, "Robust DMR and multi-rate adaptive beamforming," in *IEEE Proc. 31st Asilomar Conf. Signals, Syst. Comput.*, Pacific Grove, CA, Nov. 1997, pp. 920–924.

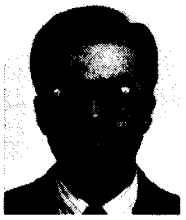

H. Song (M'02) received the B.S. and M.S. degrees in marine engineering and naval architecture from Seoul National University, Seoul, Korea, in 1978 and 1980, respectively, and the Ph.D. degree in ocean engineering from the Massachusetts Institute of Technology, Cambridge, MA, in 1990.

From 1991 to 1995, he was with Korea Ocean Research and Development Institute, Ansan. Since 1996, he has been a member of the scientists of the Marine Physical Laboratory/Scripps Institution of Oceanography, University of California, San Diego. His research interests include time-reversed acoustics, robust matched-field processing, and wave-propagation physics.

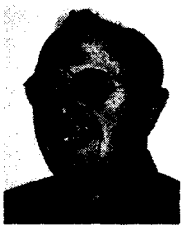

W. A. Kuperman was with the Naval Research Laboratory, the SACLANT Undersea Research Centre, La Spezia, Italy, and most recently the Scripp Institution of Oceanography of the University of California, San Diego, where he is a Professor and Director of its Marine Physical Laboratory. He has conducted theoretical and experimental research in ocean acoustics and signal processing.

W. S. Hodgkiss (S'68–M'75) was born in Bellefonte, PA, on August 20, 1950. He received the B.S.E.E. degree from Bucknell University, Lewisburg, PA, in 1972 and the M.S. and Ph.D. degrees in electrical engineering from Duke University, Durham, NC, in 1973 and 1975, respectively.

From 1975 to 1977, he was with the Naval Ocean Systems Center, San Diego, CA. From 1977 to 1978, he was a faculty member in the Electrical Engineering Department, Bucknell University. Since 1978, he has been a member of the faculty of the Scripps Institution of Oceanography, University of California, San Diego, and on the staff of the Marine Physical Laboratory. Currently, he is Deputy Director, Scientific Affairs, Scripps Institution of Oceanography. His present research interests include areas of signal processing, propagation modeling, and environmental inversions with applications of these to underwater acoustics and electromagnetic wave propagation.

Dr. Hodgkiss is a Fellow of the Acoustical Society of America.

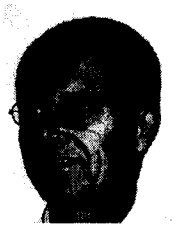

Peter Gerstoft received the M.Sc. degree from the Technical University of Denmark, Lyngby, Denmark, in 1983, the M.Sc. degree from the University of Western Ontario, London, Canada, in 1984, and the Ph.D. degree from Technical University of Denmark in 1986.

From 1987 to 1992, he was with Odegaard anDanneskiold-Samse, Copenhagen, Denmark, where he was involved with forward modeling and inversion for seismic exploration. From 1989 to 1990, he also was Visiting Scientist at the Massachusetts Institute of Technology, Cambridge. From 1992 to 1997, he was a Senior Scientist at SACLANT Undersea Research Centre, La Spezia, Italy, where he developed the SAGA inversion code, which is used for ocean acoustic and electromagnetic signals. Since 1997, he has been with Marine Physical Laboratory, University of California, San Diego. His research interests include global optimization and the modeling and inversion of acoustic, elastic, and electromagnetic signals.

Dr. Gerstoft is a Fellow of the Acoustical Society of America.

Jea Soo Kim received the B.S. degree from Seoul Nation University, Seoul, Korea, in 1981, the M.S. degree from University of Florida, Gainsville, in 1984, and the Ph.D. degree from Massachusetts Institute of Technology, Cambridge, in 1989.

Since 1991, he was with Korea Maritime University, Pusan, Korea. From 1999 to 2001, he was a Visiting Scholar in MPL/SIO, University of California, San Diego.

Source : IEEE Journal of Oceanic Engineering(2003), 28(2): 250-261